

1 **Photoenhanced sulfates formation by the heterogeneous uptake of SO₂ on non-**
2 **photoactive mineral dust**

3 Wangjin Yang, Jiawei Ma, Hongxing Yang, Fu Li, Chong Han*

4 School of Metallurgy, Northeastern University, Shenyang, 110819, China

5 *Address correspondence to author: hanch@smm.neu.edu.cn

6

7 **Short summary.** We provide evidence that light enhances the conversion of SO₂ to sulfates on
8 non-photoactive mineral dust, where triplet states of SO₂ (³SO₂) can act as a pivotal trigger to
9 generate sulfates. Photochemical sulfate formation depends on H₂O, O₂, and basicity of mineral
10 dust. The SO₂ photochemistry on non-photoactive mineral dust contributes to sulfates,
11 highlighting previously unknown pathways to better explain the missing sources of
12 atmospheric sulfates.

13

14 **Abstract.** Heterogeneous uptake of SO₂ on mineral dust is a predominant formation pathway
15 of sulfates, whereas the contribution of photo-induced SO₂ oxidation to sulfates on the dust
16 interfaces still remains unclear. Here, we investigated heterogeneous photochemical reactions
17 of SO₂ on five mineral oxides (SiO₂, kaolinite, Al₂O₃, MgO, and CaO) without photocatalytic
18 activity. Light enhanced the uptake of SO₂, and its enhancement effects negatively depended
19 on the basicity of mineral oxides. The initial uptake coefficient ($\gamma_{0, \text{BET}}$) and the steady-state
20 uptake coefficient ($\gamma_{s, \text{BET}}$) of SO₂ positively relied on light intensity, relative humidity (RH)
21 and O₂ content, while they exhibited a negative relationship with the initial SO₂ concentration.
22 Rapid sulfate formation during photo-induced heterogeneous reactions of SO₂ with all mineral
23 oxides was confirmed to be ubiquitous, and H₂O and O₂ played key roles in the conversion of
24 SO₂ to sulfates. Specially, triplet states of SO₂ (³SO₂) were suggested to be the trigger for
25 photochemical sulfate formation. Atmospheric implications supported a potential contribution
26 of interfacial SO₂ photochemistry on non-photoactive mineral dust to atmospheric sulfate
27 sources.

28

29 **Keywords:** SO₂; Sulfates; Non-photoactive mineral dust; Heterogeneous photochemistry

30

31

32 **1 Introduction**

33 As an important trace gas in the atmosphere, SO₂ is mainly emitted by volcanic eruption and
34 fuel combustion. There is an uneven distribution of atmospheric SO₂ concentrations that show
35 a distinctive seasonal and regional differentiation. Typical mixing ratios of SO₂ in the
36 troposphere are below 0.5 ppb for clean weather days, rising to several hundred ppb during
37 polluted days in urban regions (Ma et al., 2020). About half of SO₂ is oxidized to sulfate (He
38 et al., 2012), which is a key component of fine particulates in the atmosphere. High sulfate
39 loading in PM_{2.5} was observed (Shao et al., 2019), especially in polluted regions where high-
40 sulfur fuels are usually used (Olson et al., 2021). They significantly alter physicochemical
41 properties of aerosols in terms of hygroscopicity, acidity and light absorption (Chan and Chan,
42 2003; Cao et al., 2013; Lim et al., 2018). Sulfates may lead to negative health outcomes, such
43 as respiratory illness and cardiovascular (Shiraiwa et al., 2017). In addition, the deposition of
44 sulfates leads to adverse effects on ecosystems via the acidification of soils and lakes
45 (Golobokova et al., 2020). Therefore, the oxidation of SO₂ to form sulfates has attracted
46 widespread attention in the past decades.

47 The conversion of SO₂ to sulfates in the atmosphere usually occurs in different phases: gas-
48 phase oxidation of SO₂ by hydroxyl radicals (\bullet OH) or Criegee intermediate radicals (Mauldin
49 et al., 2012; Davis et al., 1979); aqueous-phase reaction of SO₂ with O₃, peroxides or transition
50 metal ions dissolved in cloud and fog droplets (Alexander et al., 2009; Herrmann et al., 2000;
51 Harris et al., 2013; Liu et al., 2020a; Li et al., 2020); and heterogeneous SO₂ uptake on aerosols
52 including authentic mineral dust, soot, inorganic ion and organic compounds (Adams et al.,
53 2005; He et al., 2018a; Ye et al., 2018; Wang et al., 2019; Yao et al., 2019; Zhang et al., 2020a;
54 Liu et al., 2020; Liu et al., 2021). However, the oxidation of SO₂ in gas and aqueous phases
55 fails to explain high sulfate concentrations in the polluted areas. Model simulation suggests

56 that the rapid sulfate formation can be attributed to the heterogeneous SO₂ uptake (Li et al.,
57 2017). A positive relationship between the fraction of sulfates and mineral dust in haze days
58 has been reported, implying that mineral dust may account for the formation of sulfates (Wang
59 et al., 2020a). Moreover, a large amount of sulfates was observed to be formed on the surface
60 of mineral dust after long-distance transport (Prospero, 1999). Thus, investigating the
61 heterogeneous oxidation of SO₂ on mineral dust can provide basic data for the model
62 calculation to evaluate atmospheric sulfates.

63 Mineral dust, as the dominant component of particulate matters in the atmosphere, accounts
64 for about 30%–60% mass fractions of global aerosols (Dentener et al., 1996; Peng et al., 2012).
65 It primarily contains SiO₂ (40%–80%), followed by Al₂O₃ (10%–15%), Fe₂O₃ (6%–13%),
66 CaO (3%–10%), MgO (1%–7%) and TiO₂ (0.1%–5%) (Urupina et al., 2021; Urupina et al.,
67 2019; Usher et al., 2003). Mineral dust can provide active sites for the adsorption and reaction
68 of gases. Up to now, the heterogeneous SO₂ uptake on authentic mineral aerosols and model
69 mineral oxides has been widely reported (Ma et al., 2019; Goodman et al., 2001; Wang et al.,
70 2018; Wang et al., 2020b), with the uptake coefficient (γ) of SO₂ varying from 10⁻⁹ to 10⁻⁴
71 (Urupina et al., 2019; Usher et al., 2002).

72 It was recognized that light could significantly enhance the heterogeneous conversion of SO₂
73 to sulfates on the surface of photocatalytic mineral dust (Chen et al., 2021; Li et al., 2019; Wang
74 et al., 2020b). Electron-hole pairs are produced via photo-induced electrons from the valence
75 band to the conduction band of photocatalytic metal oxides, and then react with H₂O and O₂ to
76 generate reactive oxygen species (ROS), such as •OH and •O₂⁻ (Chu et al., 2019). Sulfates are
77 produced by the heterogeneous reactions of SO₂ with ROS (Park and Jang, 2016; Park et al.,
78 2017; Langhammer et al., 2020; Bounechada et al., 2017). In particular, due to the large
79 abundance of non-photoactive mineral dust (more than 85% mass of total mineral dust in the
80 atmosphere) (Usher et al., 2003; Liu et al., 2022), revealing the photooxidation processes of
81 SO₂ on these mineral dust is of great importance to better reevaluate the sulfate formation on
82 aerosols in the global scale.

83 Hence, photochemical SO₂ uptake and sulfate formation on non-photoactive mineral oxides

84 were investigated using a flow reactor and an *in situ* diffuse reflectance infrared Fourier
85 transform spectroscopy (DRIFTS). The SO₂ conversion to sulfates was examined under various
86 conditions, and the roles of light intensity, SO₂ concentration, H₂O, O₂ and basicity of mineral
87 oxides were determined. Reaction mechanisms and atmospheric implications were proposed,
88 highlighting an important pathway accounting for the photochemical uptake of SO₂ to form
89 sulfates on the non-photoactive surfaces.

90

91 **2 Experimental methods**

92 **2.1 Materials**

93 Analytical grade SiO₂ (Sinopharm Chemical Reagent Co., Ltd.), kaolinite (Sinopharm
94 Chemical Reagent Co., Ltd.), Al₂O₃ (Alfa Aesar), MgO (Sigma-Aldrich), and CaO (Sigma-
95 Aldrich) were used in the experiments. Through the nitrogen Brunauer-Emmett-Teller (BET)
96 physisorption analysis, their specific surface areas were detected to be 0.419, 6.407, 8.137,
97 10.948 and 6.944 m² g⁻¹, respectively. With BaSO₄ used as the reference, the ultraviolet-visible
98 (UV-vis) light absorption spectra of samples (Figure S1) in the wavelength range of 300–800
99 nm were obtained by the Shimadzu UV-2550 spectrophotometer, which was equipped with
100 diffuse reflection integrating sphere attachment. The solid powder (0.2–5 g) was uniformly
101 dispersed into 10.0 mL ethanol solution. The mixed liquid was poured into a rectangle quartz
102 sample dish (14.0 cm × 7.0 cm) and dried to form a solid coating in an oven at 353 K for 10 h.
103 SO₂ standard gas (50 ppm in N₂, Shenyang Air Liquide Co., LTD) and high purity N₂ and O₂
104 (99.999 vol.%, Shenyang Air Liquide Co., LTD) were used as received. The solid sample
105 powder (0.2 g) was immersed in 10 mL deionized water (20 mg mL⁻¹), and then the suspension
106 was vigorously stirred for 10 min. The pH of SiO₂, kaolinite, Al₂O₃, MgO and CaO suspension
107 was measured to be 6.27, 6.58, 9.33, 10.61 and 12.72 using a pH meter, respectively.

108 **2.2 Rectangular flow reactor**

109 The uptake experiments of SO₂ on mineral dust were performed in a horizontal rectangular
110 flow reactor (26.0 cm length × 7.5 cm width × 2.0 cm height), which was depicted in Figure
111 S2. In a previous study, a similar rectangular flow reactor was designed and the feasibility of

112 the reactor has been verified (Knopf et al., 2007). The reactor was made of quartz to allow the
113 transmission of light. The temperature was maintained at 298 K by circulating temperature-
114 controlled water through the outer jacket of the reactor. Synthetic air with a N₂/O₂ volume ratio
115 of 4:1 was introduced into the flow reactor, and its total flow rate was 1000 mL min⁻¹. The
116 Reynolds number (*Re*) was calculated to be 28.2 (*Re* < 200), as described in the Supporting
117 Information, indicating a laminar flow state. SO₂ together with high purity N₂ (100 mL min⁻¹)
118 was introduced into the reactor through a movable T-shaped injector equipped with six exit
119 holes (0.2 mm diameter), so that the gas could be uniformly distributed over the width of the
120 reactor. The SO₂ concentration was 40–200 ppb and measured with a SO₂ analyzer (Thermo
121 43i). Wet N₂ generated with a bubbler containing deionized water was introduced by two
122 parallel inlets on the side of a T-shaped injector. Relative humidity (RH, 10%–75%) was
123 controlled by regulating the ratio of dry N₂ to wet N₂ and measured via a hygrometer (Center
124 314). The equivalent layer numbers of water on surface was 0.9–4.0 according to the Brunauer-
125 Emmett-Teller (BET) model (Sumner et al., 2004), and the thickness of the film of adsorbed
126 water varied between 2.7–12 nm at RH=10%–75%. There were three equally spaced exhaust
127 ports to mitigate the outlet turbulence. A xenon lamp (CEL-LAX500, China Education Au-light
128 Co., Ltd) was used to simulate sunlight and vertically located above the reactor. A filter was
129 placed on the reactor to remove the light with wavelengths shorter than 300 nm. The spectrum
130 irradiance of the xenon lamp was displayed in Figure S3 and measured using a calibrated
131 spectroradiometer (ULS2048CL-EVO, Avantes). The spectral irradiance was measured inside
132 the reactor, after passing the water cooling and in the absence of a sample. The total irradiance
133 ($0-7.93 \times 10^{16}$ photons cm⁻² s⁻¹) on the coating can be adjusted by varying the distance of the
134 xenon lamp to the reactor.

135 **2.3 Uptake coefficient of SO₂**

136 The heterogeneous reaction kinetics of SO₂ with mineral dust can be described by a pseudo-
137 first-order reaction. Figure S4 showed a linear relationship between the natural logarithm of
138 the SO₂ concentration and the reaction time. The apparent rate constant ($k_{\text{obs, SiO}_2}$) of SO₂ with
139 SiO₂ can be calculated using equation 1,

140
$$\frac{\ln(C_0/C_t)}{t} = k_{\text{obs, SiO}_2} \quad (1)$$

141 where C_0 and C_t (ppb) are the initial SO₂ concentration and the SO₂ concentration, respectively;
 142 t was calculated by dividing the length of the reactive surface by the average flow velocity. The
 143 loss of SO₂ on the internal wall of the reactor in blank experiments was carried out under
 144 various conditions (Figure S5 as an example), and it has been deducted for the γ calculation.
 145 Assuming that the wall loss was constant in the experiments with and without samples, the
 146 geometric uptake coefficient (γ_{geo}) was determined by equation 2 (Knopf et al., 2007),

147
$$\gamma_{\text{geo}} = \frac{4Vk}{S\omega} \quad (2)$$

148 where k (s⁻¹), V (4×10^{-4} m³), S (9.8×10^{-3} m²) and ω (314.05 m s⁻¹) are the reaction rate
 149 constant, the volume of the rectangular reactor, the surface area of the sample dish, and the
 150 mean molecular speed of SO₂, respectively.

151 The uptake process of SO₂ on SiO₂ depended on the reaction of SO₂ with SiO₂ and the mass
 152 transport of SO₂ to the surface. It can be expressed by equation 3,

153
$$k'_{\text{r, SiO}_2} = \left[\frac{1}{k_{\text{obs, SiO}_2} - k_{\text{obs, wall}}} - \frac{a}{N_u D} \right]^{-1} \quad (3)$$

154 where $k_{\text{obs, SiO}_2}$ and $k_{\text{obs, wall}}$ (s⁻¹) are the apparent rate constants measured with and without
 155 SiO₂ samples, respectively. $k'_{\text{r, SiO}_2}$ is the reaction rate constant of SO₂ accounting for the
 156 diffusion effect; D (0.1337 cm² s⁻¹) is the diffusion coefficient of SO₂ in air; a (1 cm) is one
 157 half height of the flow reactor; N_u is the Nusselt numbers obtained with a calculation method
 158 from Solbrig and Gidaspow (1967), which represents the mass transport. Then, the corrected γ
 159 can be calculated by equation 2 where k was replaced by $k'_{\text{r, SiO}_2}$. In our experiments, the
 160 correction for γ was estimated to be 10%. Initial uptake coefficients (γ_0) and steady-state uptake
 161 coefficients (γ_s) were calculated by averaging the signals within the 1.0 and 40–60 min reaction
 162 time, respectively.

163 To understand the diffusion depth of SO₂ and determine the interaction of SO₂ with the
 164 underlying layers of SiO₂, the uptake of SO₂ as a function of the SiO₂ mass under irradiation
 165 was shown in Figure S6. The γ exhibited a linear increase in the SiO₂ mass range of 0.05–2.0

166 g, while it remained unchanged at the SiO₂ mass > 3.0 g. Therefore, the uptake coefficient of
167 SO₂ in the linear regions was normalized using the BET surface area of SiO₂ by equation 4
168 (Brunauer et al., 1938),

$$169 \gamma_{\text{BET}} = \frac{S_{\text{geo}} \times \gamma_{\text{geo}}}{S_{\text{BET}} \times m_{\text{SiO}_2}} \quad (4)$$

170 where γ_{BET} is the SO₂ uptake coefficient normalized to the BET surface area; S_{geo} (9.8×10^{-3}
171 m²) is the geometric area of the sample dish; S_{BET} (0.419 m² g⁻¹) is the BET surface area of
172 SiO₂; m_{SiO_2} (0.05–2.0 g) is the SiO₂ mass. The same method was also used to calculate the
173 uptake coefficients of SO₂ on other mineral oxides.

174 **2.4 In situ DRIFTS analysis**

175 The changes in the chemical compositions on mineral oxides in the SO₂ uptake process were
176 investigated by the Fourier transform infrared (FTIR) spectrometer (Thermo Nicolet iS50)
177 equipped with an *in situ* diffuse reflectance accessory and a mercury cadmium telluride (MCT)
178 detector. About 14 mg mineral oxides were placed into a stainless-steel cup inside the reaction
179 cell. To remove adsorbed impurities, SiO₂ was purged with a 150 mL min⁻¹ airflow (N₂/O₂
180 volume ratio = 4:1) at RH=40% for 1 h. Then, a background spectrum of unreacted samples
181 was collected. SO₂ (2 ppm) was introduced into the reaction cell, and the IR spectra was
182 recorded as a function of time at a resolution of 4 cm⁻¹ by averaging 100 scans. The light from
183 the xenon lamp (500 W) was transmitted into the DRIFTS reaction cell via a fiber. To verify
184 the role of intermediate, Ru(bpy)₃(Cl)₂ and NaHCO₃, acting as ³SO₂ and •OH scavengers
185 (Bulgakov and Safonova, 1996; Gen et al., 2019a), respectively, were mixed with SiO₂ powder
186 in an agate mortar, and the mixture was put in the reaction cell of DRIFTS.

187

188 **3 Results and discussion**

189 **3.1 Photo-enhanced uptake of SO₂**

190 Acting as the most abundant mineral oxides, SiO₂ was used to investigate the uptake
191 behaviors of SO₂. As shown in Figure 1A, when SO₂ (80 ppb) was exposed to SiO₂ in the dark,
192 the SO₂ concentration decreased to 70 ppb, and then it quickly increased and reached a steady

193 state after 20 min. Upon exposure to SiO₂ under irradiation, the SO₂ concentration exhibited a
194 greater drop than that in the dark. The deactivation of SO₂ uptake on SiO₂ was very slight after
195 20 mins under irradiation. These suggest that light can promote the heterogeneous reaction of
196 SO₂ on SiO₂. Few studies observed the photochemical uptake of SO₂ on non-photoactive
197 minerals (Xu et al., 2021; Zhang et al., 2022). When SO₂ did not contact with SiO₂, its
198 concentration recovered rapidly. The desorption of SO₂ was observed when SO₂ was isolated
199 from SiO₂ in the dark and under irradiation, indicating that the physical adsorption partially
200 contributed to the SO₂ loss during the photochemical process. The proportion of the desorbed
201 SO₂ during the uptake process can be quantified by dividing the integral of reversible
202 desorption of SO₂ ($t = 80\text{--}100$ min) into the integral of the SO₂ uptake ($t = 20\text{--}80$ min), which
203 was calculated to be 95% and 12% in the dark and under irradiation, respectively. This implies
204 that SO₂ uptake in the dark was primarily ascribed to the physical adsorption of SO₂, while SO₂
205 uptake under irradiation was mainly attributed to chemical processes or irreversible adsorption.

206 The uptake coefficients of SO₂ on SiO₂ as a function of irradiation intensity were shown in
207 Figure 1B. The errors in all figures are the standard deviations of three repetitive experiments.
208 Both $\gamma_{0, \text{BET}}$ and $\gamma_{s, \text{BET}}$ displayed a well linear relationship with the irradiation intensity. **The**
209 **$\gamma_{0, \text{BET}}$ and $\gamma_{s, \text{BET}}$ under the irradiation of 7.93×10^{16} photons $\text{cm}^{-2} \text{s}^{-1}$ were 1.75 and 2.25 times**
210 **of those in the dark, respectively.** This further confirms the photochemical nature of the
211 reactions of SO₂ on SiO₂. In particular, $\gamma_{0, \text{BET}}$ and $\gamma_{s, \text{BET}}$ on SiO₂ under simulated solar
212 irradiation was comparable with those ($10^{-7}\text{--}10^{-6}$) on Gobi Desert dust (GDD) and Arizona
213 Test Dust (ATD) under UV irradiation, which contained photocatalytic metal oxides (Park et
214 al., 2017). As for the SO₂ uptake on TiO₂, $\gamma_{0, \text{BET}}$ and $\gamma_{s, \text{BET}}$ were measured to be 10^{-6} and 10^{-7} ,
215 respectively, by using the flow tube (Ma et al., 2019), which were similar to our results. It
216 should be pointed out that the similar uptake coefficient did not mean the comparable ability
217 of photoactive and non-photoactive mineral oxides to SO₂ uptake, since the uptake coefficient
218 was highly dependent on environmental conditions (SO₂ concentration, relative humidity,
219 mineral oxides mass, light source and pressure) and reactor type (chamber and flow tube

220 reactor). Table S1 shows that the fraction of SiO₂ in the sample was 99.02%, accompanied by
 221 a small amount of Al₂O₃, K₂O, Fe₂O₃ and CaO. Photoactive substances (Fe₂O₃) was very few
 222 in the sample, and they should not be the main contributor to the photochemical uptake of SO₂.

223 Figure 1C shows the evolution of $\gamma_{0,BET}$ and $\gamma_{s,BET}$ at different SO₂ concentrations under
 224 irradiation. An inverse dependence of $\gamma_{0,BET}$ and $\gamma_{s,BET}$ on the SO₂ concentration was observed,
 225 meaning that the efficiency of SO₂ uptake decreased with increasing the SO₂ concentration.
 226 The uptake of gases on the solid surfaces usually follows the Langmuir-Hinshelwood (L-H)
 227 mechanism (Ammann et al., 2003; Zhang et al., 2020b), suggesting that gaseous molecules are
 228 quickly absorbed on the surfaces, and then the reactions occur among the absorbed species.

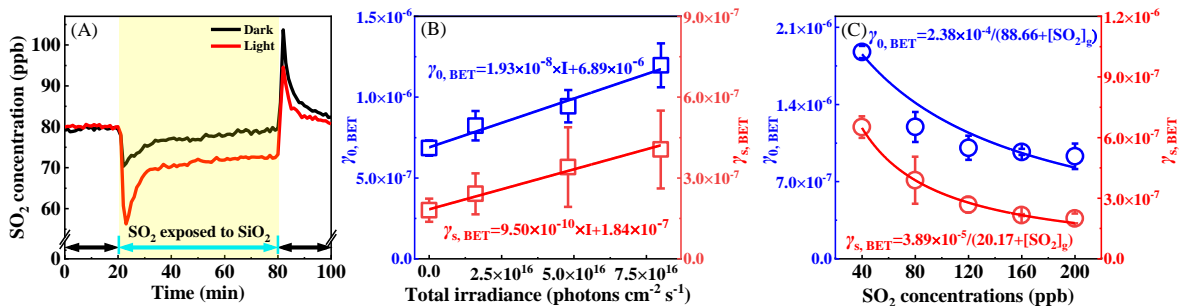
229 Assuming that the adsorption of SO₂ on SiO₂ is in accord with the Langmuir isotherm, the
 230 dependence of γ on the SO₂ concentration can be described by equation 5 (Zhang et al., 2020b),

$$231 \gamma = \frac{(4V/S\omega)k[\text{SiO}_2]_T K_{\text{SO}_2}}{1 + K_{\text{SO}_2}[\text{SO}_2]_g} \quad (5)$$

232 where $[\text{SO}_2]_g$ is the concentration of gaseous SO₂; $[\text{SiO}_2]_T$ is the total number of active sites
 233 on SiO₂; k is the reaction rate constant of SO₂ absorbed on SiO₂; K_{SO_2} represents the Langmuir
 234 adsorption constant of SO₂. Because the SiO₂ mass remained constant during the reaction,
 235 equation 5 can be written as equation 6,

$$236 \gamma = \frac{a}{1 + K_{\text{SO}_2}[\text{SO}_2]_g} \quad (6)$$

237 where $a = (4V/S\omega)k[\text{SiO}_2]_T K_{\text{SO}_2}$. As shown in Figure 1C, equation 6 can well describe the
 238 correlation of the SO₂ uptake coefficient with the SO₂ concentration, suggesting that the L-H
 239 mechanism can explain the influence of the SO₂ concentration on $\gamma_{0,BET}$ and $\gamma_{s,BET}$.

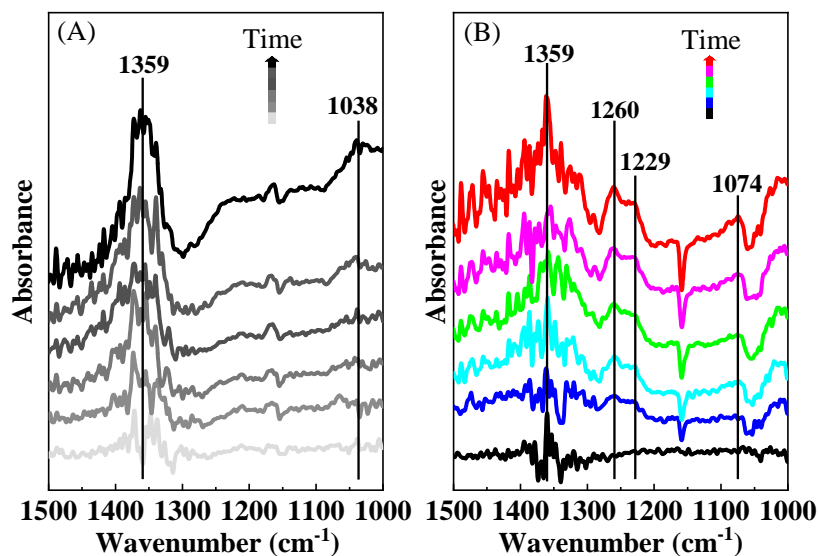


240
 241 **Figure 1.** (A) The temporal variation of the SO₂ concentration on SiO₂ in the dark and under

242 irradiation (7.93×10^{16} photons $\text{cm}^{-2} \text{s}^{-1}$); The background changes of the SO_2 concentration
243 in the blank reactor have been deducted. (B) The $\gamma_{0, \text{BET}}$ and $\gamma_{\text{s, BET}}$ of SO_2 on SiO_2 as a
244 function of the light intensity. (C) The $\gamma_{0, \text{BET}}$ and $\gamma_{\text{s, BET}}$ of SO_2 on SiO_2 at different SO_2
245 concentrations under irradiation (7.93×10^{16} photons $\text{cm}^{-2} \text{s}^{-1}$); The fitting lines for $\gamma_{0, \text{BET}}$
246 and $\gamma_{\text{s, BET}}$ were based on the Langmuir-Hinshelwood mechanism using equation 6. Reaction
247 conditions: SiO_2 mass of 0.2 g, temperature of 298 K, RH of 40% and O_2 content of 20%.

248 **3.2 Photo-induced formation of sulfates by the SO_2 uptake**

249 To investigate the products formed on SiO_2 , *in situ* DRIFTS spectra were recorded, as shown
250 in Figure 2. The band at 1359 cm^{-1} was assigned to physically-adsorbed SO_2 on SiO_2 (Urupina
251 et al., 2019). The bidentate sulfate and bisulfate contributed to the bands at 1260 and 1229/1074
252 cm^{-1} (Urupina et al., 2019; Yang et al., 2020), respectively. The bands at 1038 cm^{-1} may be
253 related to the monodentate sulfite (Yang et al., 2019; Wang et al., 2019). It was noted that the
254 intensity of physically-absorbed SO_2 (1359 cm^{-1}) under irradiation was lower than that in the
255 dark (Figure S7), which may be ascribed to further conversion of SO_2 absorbed on SiO_2 under
256 irradiation. Especially, the sulfate bands (1260, 1229 and 1074 cm^{-1}) only appeared under
257 irradiation, while the sulfites (1038 cm^{-1}) were only detected in the dark. This suggests that
258 light changed the SO_2 conversion pathways on SiO_2 . As shown in Figure S7, the bands at
259 $1157/1055 \text{ cm}^{-1}$ were assigned to the asymmetric stretching of Si-O (Hu et al., 2003). Sulfate
260 generated on the surface may interact with SiO_2 , leading to a decrease in the intensity of peaks
261 ($1157/1055 \text{ cm}^{-1}$).



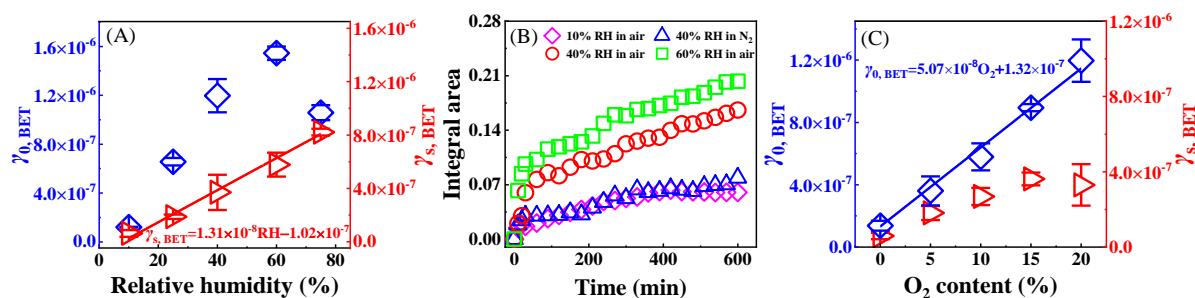
262

263 **Figure 2.** *In situ* DRIFTS spectra of SiO₂ during the uptake process of SO₂ (2 ppm) in the
 264 dark (A) and under irradiation (B). Reaction conditions: RH of 40%, temperature of 298 K
 265 and O₂ content of 20%.

266 3.3 Key roles of H₂O and O₂ in photochemical conversion of SO₂ to sulfates

267 Figure S8A shows temporal variations of the SO₂ concentration in the reaction with SiO₂ at
 268 RH=10% and 60% under irradiation. The uptake of SO₂ was very weak at RH=10%, whereas
 269 it was obvious at RH=60%. Moreover, H₂O prolonged the time to reach the steady-state uptake
 270 of SO₂. This means that H₂O plays an enhancement role in the photochemical uptake of SO₂.
 271 As shown in Figure 3A, $\gamma_{0, \text{BET}}$ had a continuous increase from $(1.20 \pm 0.04) \times 10^{-7}$ to $(1.54 \pm$
 272 $0.07) \times 10^{-6}$ with increasing the RH in the 10%–60% range, but it decreased to $(1.05 \pm 0.09) \times$
 273 10^{-6} at RH=75%. The $\gamma_{s, \text{BET}}$ linearly depended on the RH, and linear fitting to $\gamma_{s, \text{BET}}$ versus
 274 RH yielded an equation $\gamma_{s, \text{BET}} = 1.31 \times 10^{-8} \times \text{RH} - 1.02 \times 10^{-7}$. Adsorbed H₂O promoted the
 275 hydration and dissociation of SO₂ (Huang et al., 2015), and it may generate reactive oxygen
 276 species (ROS) such as •OH or HO₂ radicals to oxidize SO₂ under irradiation (Li et al., 2020;
 277 Ma et al., 2019), which would lead to positive effects of RH on the SO₂ uptake. Adsorbed H₂O
 278 also occupied adsorptive and active sites on the surface, leading to a decrease in SO₂ adsorption.
 279 When this competitive role was dominated, the uptake of SO₂ would be hindered.

280 The DRIFTS spectra of SiO₂ during the SO₂ uptake at different RHs are shown in Figure
 281 S9A. The band intensities of sulfates (1260 and 1229 cm⁻¹) at RH=60% were stronger than
 282 those at RH=10%, suggesting that H₂O promotes the sulfate formation. To further investigate
 283 the influence of H₂O on the sulfate formation, the integrated area of sulfates in the DRIFTS
 284 spectra (1289–1202 cm⁻¹) as a function of the time at different RHs is illustrated in Figure 3B.
 285 Sulfates exhibited a fast formation in the initial 30 min, and then they were continuously
 286 generated at a relatively slow rate. SO₂ absorption on the surface would be blocked because of
 287 the accumulation of H₂O and products (sulfites and sulfates), resulting in the gradual
 288 deactivation of the surface. It was noted that sulfates formation was more prominent at higher
 289 RH, revealing that H₂O can act as an important participator in the production of sulfates by the
 290 photochemical uptake of SO₂ on SiO₂.



291
 292 **Figure 3.** (A) The dependence of $\gamma_{0, \text{BET}}$ and $\gamma_{s, \text{BET}}$ on RH. (B) Integrated area of sulfates in
 293 DRIFTS spectra (1289–1202 cm⁻¹) as a function of time. (C) The dependence of $\gamma_{0, \text{BET}}$ and
 294 $\gamma_{s, \text{BET}}$ on O₂. Reaction conditions: SiO₂ mass of 0.2 g, irradiation intensity of 7.93×10^{16}
 295 photons cm⁻² s⁻¹, temperature of 298 K, O₂ content of 20% for (A) and RH of 40% for (B).

296 Figure S8B displays effects of O₂ on the photochemical uptake of SO₂ on SiO₂. Negligible
 297 SO₂ uptake occurred in N₂, while there was a significant decrease in the SO₂ concentration in
 298 air. The $\gamma_{0, \text{BET}}$ greatly increased from $(1.37 \pm 0.45) \times 10^{-7}$ under anaerobic condition to $(1.19$
 299 $\pm 0.13) \times 10^{-6}$ under 20% O₂ content condition (Figure 3C), confirming that O₂ was involved
 300 in the reaction of SO₂ on SiO₂. The $\gamma_{s, \text{BET}}$ increased from $(7.10 \pm 2.85) \times 10^{-8}$ under anaerobic

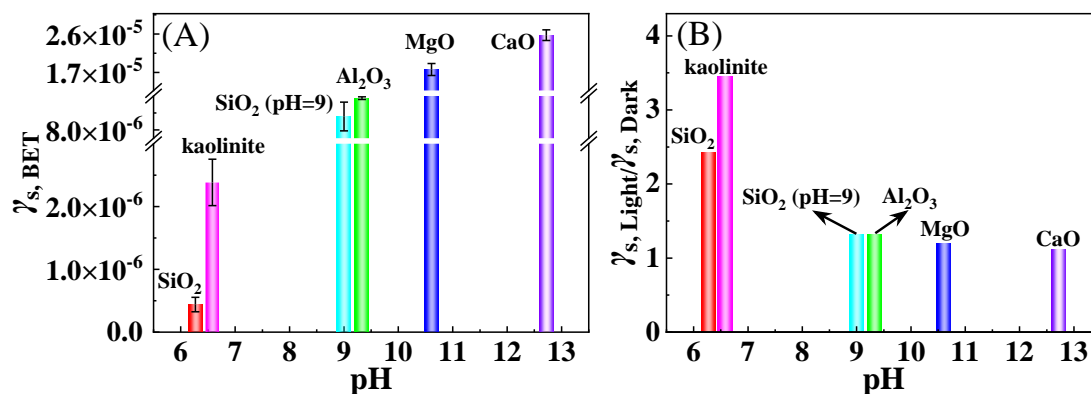
301 condition to $(4.37 \pm 0.58) \times 10^{-7}$ under 15% O₂ content condition, whereas it remained
302 unchanged with further increasing the O₂ content.

303 DRIFTS spectra of SiO₂ during the SO₂ uptake in N₂ and air were compared in Figure S9B.
304 In both air and N₂, the bands of absorbed SO₂ (1359 cm⁻¹), sulfates (1260, 1229 and 1074
305 cm⁻¹). Nevertheless, their intensities in N₂ were weaker than those in air. According to the
306 integrated area of sulfates in the DRIFTS spectra (1289–1202 cm⁻¹), the formation trends of
307 sulfates were similar in N₂ and air (Figure 3B), while the sulfate formation rate in N₂ was
308 obviously lower than that in air, meaning that O₂ enhanced the sulfate production. It was
309 reported that the production rate of sulfates from the SO₂ uptake on TiO₂ and by the photolysis
310 of nitrates under UV irradiation in N₂ was also smaller than that in air (Ma et al., 2019; Gen et
311 al., 2019b). In addition, it was noted that sulfates can be generated in N₂, meaning that O₂ was
312 not necessary and some pathways contributed to sulfates without O₂.

313 **3.4 Ubiquitously photoenhanced conversion of SO₂ to sulfates**

314 To better assess the potential for photochemical conversion of SO₂ to sulfates, the SO₂ uptake
315 experiments were further performed on typical mineral oxides without photocatalytic activity.
316 As displayed in Figure S10, more obvious SO₂ uptake on kaolinite, Al₂O₃, MgO and CaO were
317 observed under irradiation compared to those in the dark. Figure 4A shows that there was the
318 largest $\gamma_{s, \text{BET}}$ for CaO among five minerals, and $\gamma_{s, \text{BET}}$ positively depended on the basicity (pH)
319 of mineral oxides. Basic oxides generally contains more surface hydroxyls, which enhanced
320 the heterogeneous uptake of SO₂ (Zhang et al., 2006). The ratios of steady-state uptake
321 coefficients under irradiation to those in the dark ($\gamma_{s, \text{Light}}/\gamma_{s, \text{Dark}}$) were larger than 1.0 for all
322 mineral oxides (Figure 4B). The experiments for the pH dependence on SiO₂ have been also
323 performed (Figure S11). The pH of SiO₂ suspension was adjusted to pH = 9, and $\gamma_{s, \text{BET}}$ and
324 $\gamma_{s, \text{Light}}/\gamma_{s, \text{Dark}}$ were determined to be $(8.79 \pm 0.85) \times 10^{-6}$ and 1.31, respectively (Figure 4A and
325 4B). These results suggest that light can generally enhance the SO₂ uptake on minerals at a
326 wide pH range. However, the $\gamma_{\text{Light}}/\gamma_{\text{Dark}}$ had smaller values with an increase in the basicity,

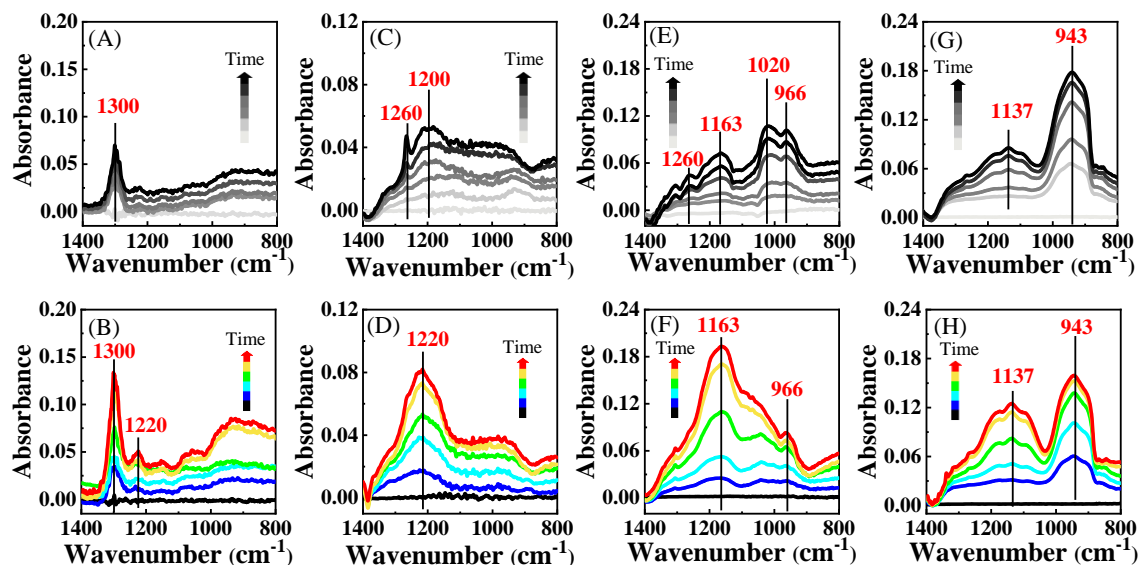
327 suggesting that the promotion effect of the light was less remarkable for basic oxides.



328

329 **Figure 4.** (A) The dependence of $\gamma_{s, \text{BET}}$ under irradiation on the basicity (pH) of mineral
 330 oxides. (B) The ratios of steady-state uptake coefficients under irradiation to those in the dark
 331 ($\gamma_{s, \text{Light}}/\gamma_{s, \text{Dark}}$). Reaction conditions: mineral oxides mass of 0.2 g, irradiation intensity of
 332 7.93×10^{16} photons $\text{cm}^{-2} \text{s}^{-1}$, temperature of 298 K, RH of 40% and O₂ content of 20%.

333 As shown in Figure 5A and B, the band at 1300 cm^{-1} should be ascribed to the sulfate. The
 334 intensity of sulfate (1300 and 1220 cm^{-1}) under irradiation was larger than those in the dark.
 335 Compared to weaker peaks of sulfates (1200 and 1260 cm^{-1}) for Al₂O₃ in the dark (Figure 5C),
 336 a stronger band of bisulfates appeared at 1220 cm^{-1} under irradiation (Figure 5D). By contrast
 337 to the generation of sulfates for kaolinite and Al₂O₃, both sulfites and sulfates formations were
 338 observed for MgO and CaO (Figure 5E–H). Sulfites were dominant in the dark, as shown by
 339 the peaks at 966 and 1020 cm^{-1} for MgO and 943 cm^{-1} for CaO, whereas the sulfate formation
 340 was significantly enhanced under irradiation according to peak intensities at 1163 cm^{-1} for
 341 MgO and 1137 cm^{-1} for CaO. It should be noted that these mineral oxides were non-
 342 photoactive because of their poor light absorption property (Figure S1). Nevertheless, the light
 343 can promote the formation of sulfates via the SO₂ uptake process on mineral oxides without
 344 photocatalytic activity.



345

346 **Figure 5.** *In situ* DRIFTS spectra of kaolinite (A and B), Al₂O₃ (C and D), MgO (E and F),
 347 CaO (G and H) during the uptake process of SO₂ (2 ppm) for 600 min in the dark (black
 348 lines) and under irradiation (colorful lines). Reaction conditions: RH of 40%, temperature of
 349 298 K and O₂ content of 20%.

350 3.5 Conversion mechanisms of SO₂ to sulfates

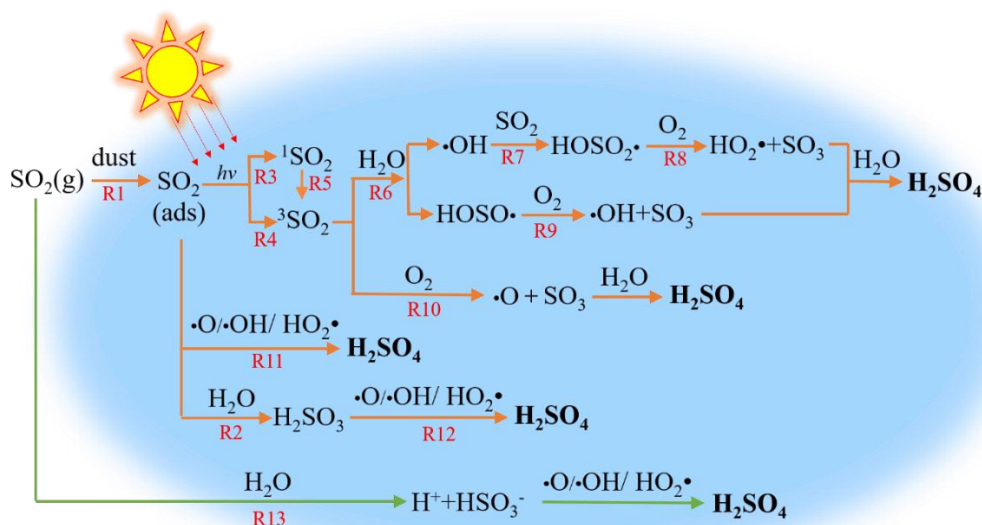
351 Heterogeneous photochemical reaction mechanisms of SO₂ on non-photoactive mineral dust
 352 were proposed in light of experimental observations (Figure 6). Gaseous SO₂ was adsorbed on
 353 the surface (R1), and then reacted with H₂O to form sulfites (R2). Under irradiation, adsorbed
 354 SO₂ accepted photons to form its singlet states (¹SO₂) and ³SO₂ (R3–5) (Sidebottom et al., 1972;
 355 Martins-Costa et al., 2018). The reaction between ³SO₂ and H₂O resulted in the formation of
 356 HOSO• and •OH (R6), which can combine with SO₂ to produce HOSO₂• (R7). HOSO• and
 357 HOSO₂• can be transformed into SO₃, which reacted with H₂O to drive the sulfate formation
 358 (R8 and R9). The interaction between ³SO₂ and O₂ may also generate SO₃ directly, which
 359 would be converted to sulfates subsequently (R10). Theoretical calculations suggested that the
 360 multistep reactions between ³SO₂ with H₂O and O₂ had small energy barriers or were barrier-
 361 free (Gong et al., 2022), which could enhance the generation of ROS and the transformation of
 362 S(IV) to S(VI). As displayed by R11 and R12, SO₂ and H₂SO₃ adsorbed on the surface may be
 363 oxidized to form sulfates via the reactions with ROS including •O, •OH or HO₂•, which were

364 produced in R6 and R8–10. In addition, gaseous SO₂ could be dissolved into adsorbed H₂O to
365 generate bisulfites, which would be finally converted to sulfates by ROS (R13) (Urupina et al.,
366 2019). As displayed in Figure S12A, the IR peaks of sulfates were not observed when tris (2,2'-
367 bipyridine) ruthenium dihydrochloride (Ru(bpy)₃(Cl)₂) was employed as the quencher of ³SO₂.
368 The peaks were assigned to the vibrations of excited Ru(bpy)₃(Cl)₂ (Mukuta et al., 2014). This
369 definitely proves that ³SO₂ is the key trigger for the sulfate formation. Figure S12B shows that
370 the peaks of sulfates were weaker in the presence of NaHCO₃, confirming the dominant
371 contribution of •OH formed in R6 and R9 to the formation of sulfates.

372 Several photochemical mechanisms have been reported to explain the sulfate formation via
373 the SO₂ uptake on various surfaces. Photoactive mineral oxides (such as TiO₂, F₂O₃ and ZnO)
374 can accept photons to produce electron-hole pairs, which generated ROS for the conversion of
375 SO₂ to sulfates (Ma et al., 2019; Li et al., 2019; Wang et al., 2020b). For example, •OH and
376 HO₂•, generated from the reaction of hole with H₂O and electron with O₂, respectively, can act
377 as oxidizing agents for the reaction with SO₂ (Ma et al., 2019). Similarly, the reaction of SO₂
378 with photo-induced •OH obviously enhanced the formation of sulfate on diesel soot and actual
379 PM_{2.5} (Zhang et al., 2022; Zhang et al., 2020c). NO₂ and NO₂⁻/HNO₂ can be formed in the
380 nitrates photolysis, and primarily contribute to the oxidation of SO₂ to sulfates on nitrates (Gen
381 et al., 2019b; Gen et al., 2019a). Theoretically, the mechanism proposed in this study should
382 also occur on photo-excited substrates. Taking TiO₂ as an example, SO₂ competed with TiO₂
383 for photons, and the production efficiency of ³SO₂ and excited state of TiO₂ (TiO₂^{*}) depended
384 on their light absorption properties. Meanwhile, ³SO₂ had a competition electron-hole pairs
385 generated from TiO₂^{*} for O₂ and H₂O. Thus, the dominant mechanism for the SO₂ uptake on
386 TiO₂ should be related to light absorption properties of precursors and the reactivity for ³SO₂
387 and TiO₂^{*} to O₂ and H₂O. By contrast, all mineral oxides used here cannot be excited under
388 irradiation according to their light absorption spectra (Figure S1). Nevertheless, SO₂ adsorbed
389 on mineral oxides can absorb the ultraviolet radiation (290–400 nm) to form the excited states
390 of SO₂ (SO₂^{*}) (Kroll et al., 2018), which subsequently reacted with H₂O and O₂, finally
391 converting SO₂ to sulfates. The SO₂ uptake experiment in the dark and the visible light (>420

392 nm) was carried out (Figure S13). An ignorable difference was observed for the SO₂
 393 concentration with or without visible light, suggesting that visible light had a minor contribution
 394 to the photoenhanced SO₂ uptake.

395 According to the experimental results, some surfaces, providing absorptive sites for SO₂, can
 396 enhance the photooxidation of SO₂ to sulfates. However, the promotion effect would vary with
 397 different substances. For example, the current experiments on some basic minerals indicate that
 398 light plays a minor enhancement role in the SO₂ uptake (Figure 4), but it could still enhance the
 399 sulfate formation (Figure 5). The solubility and effective Henry's law constant of SO₂ were
 400 positively dependent on pH. Thus, SO₂ was more liable to be dissolved to form HSO₃⁻/SO₃²⁻
 401 on more alkaline surface, leading to a strong SO₂ uptake in the dark (Figure 4A and 4B), and
 402 abundant sulfites on surfaces (Figure 5). Nevertheless, gaseous SO₂ tends to be adsorbed on
 403 kaolinite and Al₂O₃ due to less solubility of SO₂ on these surfaces, and then converted to sulfate
 404 under irradiation (Figure 6). Accordingly, a promotion effect of light on SO₂ uptake was
 405 observed on neutral and weakly alkaline surfaces (Figure 4B).



406
 407 **Figure 6.** The proposed photochemical conversion mechanisms of SO₂ to sulfates on non-
 408 photoactive mineral dust.

409 **4 Atmospheric implications**

410 The lifetime (τ) for photochemical loss of SO₂ on mineral dust was given using equation 7,

411
$$\tau = \frac{4}{\gamma\omega A} \quad (7)$$

412 where γ and ω are the uptake coefficient and the mean molecular speed of SO₂, respectively; A
 413 is the surface area density of mineral dust, and it is estimated to be $(1.4\text{--}4.8) \times 10^{-5} \text{ cm}^2 \text{ cm}^{-3}$
 414 (Zhang et al., 2019; He et al., 2018b). In this work, $\gamma_{s, \text{BET}}$ of SO₂ on several mineral oxides
 415 were measured to be 4.39×10^{-7} – 3.45×10^{-5} (Reaction conditions: SO₂ concentration of 40
 416 ppb, irradiation intensity of $7.93 \times 10^{16} \text{ photons cm}^{-2} \text{ s}^{-1}$ and RH of 40%). Thus, the τ of SO₂
 417 with respect to the photooxidation on mineral dust was calculated to be 0.9–240 days, which
 418 was shorter than that (54 years) for the photochemical uptake of SO₂ on TiO₂ and the
 419 corresponding one (346 days) for the heterogeneous oxidation of SO₂ on ATD in the presence
 420 of nitrates (Ma et al., 2019; Zhang et al., 2019). The reaction conditions in this study and those
 421 in the literatures are different in some respects, and the previously reported SO₂ uptake
 422 coefficient (10^{-7} – 10^{-6}) had a lower value (Ma et al., 2019). The huge difference in the τ of SO₂
 423 was also ascribed to the variation in the surface area density. The content of TiO₂ in mineral
 424 dust was only about 1%, and thus the surface area density of TiO₂ was about $10^{-7} \text{ cm}^2 \text{ cm}^{-3}$,
 425 leading to a longer τ (54 years) for SO₂ on TiO₂ (Ma et al., 2019). It was comparable to the
 426 lifetime (3.6–20 days) of SO₂ for the gas-phase reaction with $\bullet\text{OH}$ at a concentration of $\sim 10^{-6}$
 427 molecules cm^{-3} (Huang et al., 2015; Zhang et al., 2019). Therefore, the photochemical process
 428 with the excited state SO₂ acting as a driver on mineral dust was an important pathway for the
 429 SO₂ sink in the atmosphere.

430 Sulfates show significant influences on the atmosphere, such as an important contributor to
 431 the haze formation, affecting the activity of aerosols acting as cloud condensation nuclei (CCN)
 432 and ice nuclei (IN), and modifying optical property and acidity of aerosols. A sulfate formation
 433 rate (R) can be obtained using γ by equation 8 (Cheng et al., 2016),

434
$$R = \frac{d[SO_4^{2-}]}{dt} = \left[\frac{R_p}{D} + \frac{4}{\gamma\omega} \right]^{-1} A[SO_2] \quad (8)$$

435 where R_p is the radius of mineral dust, which can be estimated using equation 9 (Li et al., 2020),

436
$$R_p = (0.254 \times [PM_{2.5}]/(\mu\text{g m}^{-3}) + 10.259) \times 10^{-9} \text{ m} \quad (9)$$

437 where $[PM_{2.5}]$ was average $PM_{2.5}$ mass concentration, and $300 \mu\text{g m}^{-3}$ was used for the polluted
438 periods in typical China cities (Li et al., 2020; Guo et al., 2014). It was assumed that mineral
439 dust accounted for 50% mass of $PM_{2.5}$ (Tohidi et al., 2022), and the mass fraction of SiO_2 ,
440 Al_2O_3 , MgO , and CaO in mineral dust was 60%, 12.5%, 4% and 6.5%, respectively (Urupina
441 et al., 2021; Urupina et al., 2019; Usher et al., 2003). Thus, R was determined to be $2.15 \mu\text{g}$
442 $\text{m}^{-3} \text{h}^{-1}$. This suggests that the SO_2 uptake on non-photoactive surfaces may be an important
443 sulfate formation pathway under irradiation in some dust-rich conditions.

444

445 **Author contributions**

446 CH, WY and JM designed and conducted experiments; CH, WY and JM analyzed the data and
447 prepared the paper with contributions from HY; FL conducted experiments; CH supervised the
448 project.

449

450 **Competing interests**

451 The authors declare that they have no conflict of interest.

452

453 **Acknowledgements**

454 This work was supported by the National Natural Science Foundation of China [grant number
455 42077198], the LiaoNing Revitalization Talents Program [grant number XLYC1907185], and
456 the Fundamental Research Funds for the Central Universities [grant numbers N2325034;
457 N2025011].

458

459 **Reference**

460 Adams, J., Rodriguez, D., and Cox, R.: The uptake of SO_2 on Saharan dust: A flow tube study,
461 *Atmos. Chem. Phys.*, 5, 2679-2689, <https://doi.org/10.5194/acpd-5-2643-2005>, 2005.
462 Alexander, B., Park, R. J., Jacob, D. J., and Gong, S.: Transition metal-catalyzed oxidation of
463 atmospheric sulfur: Global implications for the sulfur budget, *J. Geophys. Res.*, 114, 2309-
464 2312, <https://doi.org/10.1029/2008jd010486>, 2009.
465 Ammann, M., Poschl, U., and Rudich, Y.: Effects of reversible adsorption and Langmuir-
466 Hinshelwood surface reactions on gas uptake by atmospheric particles, *Phys. Chem. Chem.*

467 Phys., 5, 351-356, <https://doi.org/10.1039/b208708a>, 2003.

468 Bounechada, D., Anderson, D., Skoglundh, M., and Carlsson, P.: SO₂ adsorption on silica
469 supported iridium, *J. Chem. Phys.*, 146, 084701-084708, <https://doi.org/10.1063/1.4976835>,
470 2017.

471 Brunauer, B., Deming, L., Deming, W., and Teller, E.: Adsorption of gases in multimolecular
472 layers, *J. Am. Chem. Soc.*, 60, 309-319, <https://doi.org/10.1021/ja01269a023>, 1938.

473 Bulgakov, R. G. and Safonova, L. A.: Chemiluminescence in the oxidation of Na₂S by oxygen
474 in water solutions, *Russ. Chem. Bull.*, 45, 1775-1776, <https://doi.org/10.1007/bf01431827>,
475 1996.

476 Cao, J., Tie, X., Dabberdt, W. F., Jie, T., Zhao, Z., An, Z., Shen, Z., and Feng, Y.: On the
477 potential high acid deposition in northeastern China, *J. Geophys. Res.: Atmos.*, 118, 4834-
478 4846, <https://doi.org/10.1002/jgrd.50381>, 2013.

479 Chan, M. and Chan, C.: Hygroscopic properties of two model humic-like substances and their
480 mixtures with inorganics of atmospheric importance, *Environ. Sci. Technol.*, 37, 5109-5115,
481 <https://doi.org/10.1021/es034272o>, 2003.

482 Chen, Y., Tong, S., Li, W., Liu, Y., Tan, F., Ge, M., Xie, X., and Sun, J.: Photocatalytic oxidation
483 of SO₂ by TiO₂: Aerosol formation and the key role of gaseous reactive oxygen species,
484 *Environ. Sci. Technol.*, 55, 9784-9793, <https://doi.org/10.1021/acs.est.1c01608>, 2021.

485 Cheng, Y., Zheng, G., Wei, C., Mu, Q., Zheng, B., Wang, Z., Gao, M., Zhang, Q., He, K.,
486 Carmichael, G., Pöschl, U., and Su, H.: Reactive nitrogen chemistry in aerosol water as a
487 source of sulfate during haze events in China, *Sci. Adv.*, 2, 1601530-1601540,
488 <https://doi.org/10.1126/sciadv.1601530>, 2016.

489 Chu, B., Wang, Y. L., Yang, W. W., Ma, J. Z., Ma, Q. X., Zhang, P., Liu, Y. C., and He, H.:
490 Effects of NO₂ and C₃H₆ on the heterogeneous oxidation of SO₂ on TiO₂ in the presence or
491 absence of UV-Vis irradiation, *Atmos. Chem. Phys.*, 19, 14777-14790,
492 <https://doi.org/10.5194/acp-19-14777-2019>, 2019.

493 Davis, D. D., Ravishankara, A. R., and Fischer, S.: SO₂ oxidation via the hydroxyl radical:
494 Atmospheric fate of HSO_x radicals, *Geo. Res. Lett.*, 6, 113-116,
495 <https://doi.org/10.1029/GL006i002p00113>, 1979.

496 Dentener, F., Carmichael, G., Zhang, Y., Lelieveld, J., and Crutzen, P.: Role of mineral aerosol
497 as a reactive surface in the global troposphere, *J. Geophys. Res.: Atmos.*, 101, 22869-22889,
498 <https://doi.org/10.1029/96jd01818>, 1996.

499 Gen, M., Zhang, R., Huang, D., Li, Y., and Chan, C.: Heterogeneous oxidation of SO₂ in sulfate
500 production during nitrate photolysis at 300 nm: Effect of pH, relative humidity, irradiation
501 intensity, and the presence of organic compounds, *Environ. Sci. Technol.*, 53, 8757-8766,
502 <https://doi.org/10.1021/acs.est.9b01623>, 2019a.

503 Gen, M., Zhang, R., Huang, D., Li, Y., and Chan, C.: Heterogeneous SO₂ oxidation in sulfate
504 formation by photolysis of particulate nitrate, *Environ. Sci. Tech. Lett.*, 6, 86-91,
505 <https://doi.org/10.1021/acs.estlett.8b00681>, 2019b.

506 Golobokova, L., Khodzher, T., Khuriganova, O., Marinayte, I., Onishchuk, N., Rusanova, P.,
507 and Potemkin, V.: Variability of chemical properties of the atmospheric aerosol above lake
508 baikal during large wildfires in siberia, *Atmosphere*, 11, 1230-1250,

509 <https://doi.org/10.3390/atmos11111230>, 2020.

510 Gong, C., Yuan, X., Xing, D., Zhang, D., Martins-Costa, M. T. C., Anglada, J. M., Ruiz-Lopez,
511 M. F., Francisco, J. S., and Zhang, X.: Fast sulfate formation initiated by the spin-forbidden
512 excitation of SO₂ at the air-water interface, *J. Am. Chem. Soc.*, 144, 22302-22308,
513 <https://doi.org/10.1021/jacs.2c10830>, 2022.

514 Goodman, A., Li, P., Usher, C., and Grassian, V.: Heterogeneous uptake of sulfur dioxide on
515 aluminum and magnesium oxide particles, *J. Phys. Chem. A* 105, 6109-6120,
516 <https://doi.org/10.1021/jp004423z>, 2001.

517 Guo, S., Hu, M., Zamora, M. L., Peng, J., Shang, D., Zheng, J., Du, Z., Wu, Z., Shao, M., Zeng,
518 L., Molina, M. J., and Zhang, R.: Elucidating severe urban haze formation in China, *Proc.*
519 *Natl. Acad. Sci. U. S. A.*, 111, 17373-17378, <https://doi.org/10.1073/pnas.1419604111>,
520 2014.

521 Harris, E., Sinha, B., van Pinxteren, D., Tilgner, A., Fomba, K. W., Schneider, J., Roth, A.,
522 Gnauk, T., Fahlbusch, B., Mertes, S., Lee, T., Collett, J., Foley, S., Borrmann, S., Hoppe, P.,
523 and Herrmann, H.: Enhanced role of transition metal ion catalysis during in-cloud oxidation
524 of SO₂, *Science*, 340, 727-730, <https://doi.org/10.1126/science.1230911>, 2013.

525 He, G., Ma, J., and He, H.: Role of carbonaceous aerosols in catalyzing sulfate formation, *ACS*
526 *Catal.*, 8, 3825-3832, <https://doi.org/10.1021/acscatal.7b04195>, 2018a.

527 He, H., Li, C., Loughner, C. P., Li, Z., Krotkov, N. A., Yang, K., Wang, L., Zheng, Y., Bao, X.,
528 Zhao, G., and Dickerson, R. R.: SO₂ over central China: Measurements, numerical
529 simulations and the tropospheric sulfur budget, *J. Geophys. Res.: Atmos.*, 117, 37-51,
530 <https://doi.org/10.1029/2011jd016473>, 2012.

531 He, P., Alexander, B., Geng, L., Chi, X., Fan, S., Zhan, H., Kang, H., Zheng, G., Cheng, Y., Su,
532 H., Liu, C., and Xie, Z.: Isotopic constraints on heterogeneous sulfate production in Beijing
533 haze, *Atmos. Chem. Phys.*, 18, 5515-5528, <https://doi.org/10.5194/acp-18-5515-2018>,
534 2018b.

535 Herrmann, H., Ervens, B., Jacobi, H. W., Wolke, R., Nowacki, P., and Zellner, R.: CAPRAM_{2,3}:
536 A chemical aqueous phase radical mechanism for tropospheric chemistry, *J. Atmos. Chem.*,
537 36, 231-284, <https://doi.org/10.1023/A:1006318622743>, 2000.

538 Huang, L., Zhao, Y., Li, H., and Chen, Z.: Kinetics of heterogeneous reaction of sulfur dioxide
539 on authentic mineral dust: Effects of relative humidity and hydrogen peroxide, *Environ. Sci.*
540 *Technol.*, 49, 10797-10805, <https://doi.org/10.1021/acs.est.5b03930>, 2015.

541 Hu, Q., Suzuki, H., Gao, H., Araki, H., Yang, W., and Noda, T.: High-frequency FTIR
542 absorption of SiO₂/Si nanowires, *Chem. Phys. Lett.*, 378, 299-304,
543 <https://doi.org/10.1016/j.cplett.2003.07.015>, 2003.

544 Knopf, D., Cosman, L., Mousavi, P., Mokamati, S., and Bertram, A.: A novel flow reactor for
545 studying reactions on liquid surfaces coated by organic monolayers: Methods, validation,
546 and initial results, *J. Phys. Chem. A*, 111, 11021-11032, <https://doi.org/10.1021/jp075724c>,
547 2007.

548 Kroll, J., Frandsen, B., Kjaergaard, H., and Vaida, V.: Atmospheric hydroxyl radical source:
549 Reaction of triplet SO₂ and water, *J. Phys. Chem. A*, 122, 4465-4469, [https://doi.org/10.10](https://doi.org/10.1021/acs.jpca.8b03524)
550 [21/acs.jpca.8b03524](https://doi.org/10.1021/acs.jpca.8b03524), 2018.

551 Langhammer, D., Kullgren, J., and Osterlund, L.: Photoinduced adsorption and oxidation of
552 SO₂ on anatase TiO₂, *J. Am. Chem. Soc.*, 142, 21767-21774, [https://doi.org/10.1021/jacs.0](https://doi.org/10.1021/jacs.0c09683)
553 [c09683](https://doi.org/10.1021/jacs.0c09683), 2020.

554 Li, G., Bei, N., Cao, J., Huang, R., Wu, J., Feng, T., Wang, Y., Liu, S., Zhang, Q., Tie, X., and
555 Molina, L. T.: A possible pathway for rapid growth of sulfate during haze days in China,
556 *Atmos. Chem. Phys.*, 17, 3301-3316, <https://doi.org/10.5194/acp-17-3301-2017>, 2017.

557 Li, J., Zhang, Y. L., Cao, F., Zhang, W., Fan, M., Lee, X., and Michalski, G.: Stable sulfur
558 isotopes revealed a major role of transition-metal ion-catalyzed SO₂ oxidation in haze
559 episodes, *Environ. Sci. Technol.*, 54, 2626-2634, <https://doi.org/10.1021/acs.est.9b07150>,
560 2020.

561 Li, K., Kong, L., Zhankakova, A., Tong, S., Shen, J., Wang, T., Chen, L., Li, Q., Fu, H., and
562 Zhang, L.: Heterogeneous conversion of SO₂ on nano α -Fe₂O₃: the effects of morphology,
563 light illumination and relative humidity, *Environ. Sci.: Nano*, 6, 1838-1851,
564 <https://doi.org/10.1039/c9en00097f>, 2019.

565 Lim, S., Lee, M., Kim, S., and Laj, P.: Sulfate alters aerosol absorption properties in East Asian
566 outflow, *Sci. Rep.*, 8, 5172-5178, <https://doi.org/10.1038/s41598-018-23021-1>, 2018.

567 Liu, T., Clegg, S., and Abbatt, J. P. D.: Fast oxidation of sulfur dioxide by hydrogen peroxide
568 in deliquesced aerosol particles, *Proc. Natl. Acad. Sci. U. S. A.*, 117, 1354-1359,
569 <https://doi.org/10.1073/pnas.1916401117>, 2020a.

570 Liu, T., Chan, A. W. H., and Abbatt, J. P. D.: Multiphase oxidation of sulfur dioxide in aerosol
571 particles: Implications for sulfate formation in polluted environments, *Environ. Sci.*
572 *Technol.*, 55, 4227-4242, <https://doi.org/10.1021/acs.est.0c06496>, 2021.

573 Liu, Y., Deng, Y., Liu, J., Fang, X., Wang, T., Li, K., Gong, K., Bacha, A. U., Nabi, I., Ge, Q.,
574 Zhang, X., George, C., and Zhang, L.: A novel pathway of atmospheric sulfate formation
575 through carbonate radicals, *Atmos. Chem. Phys.*, 22, 9175-9197,
576 <https://doi.org/10.5194/acp-22-9175-2022>, 2022.

577 Ma, J., Dörner, S., Donner, S., Jin, J. L., Cheng, S. Y., Guo, J. R., Zhang, Z. F., Wang, J. Q.,
578 Liu, P., Zhang, G. Q., Pukite, J., Lampel, J., and Wagner, T.: MAX-DOAS measurements of
579 NO₂, SO₂, HCHO, and BrO at the Mt. Waliguan WMO GAW global baseline station in the
580 Tibetan Plateau, *Atmos. Chem. Phys.*, 20, 6973-6990, [https://doi.org/10.5194/acp-20-6973-](https://doi.org/10.5194/acp-20-6973-2020)
581 [2020](https://doi.org/10.5194/acp-20-6973-2020), 2020.

582 Ma, Q., Wang, L., Chu, B., Ma, J., and He, H.: Contrary role of H₂O and O₂ in the kinetics of
583 heterogeneous photochemical reactions of SO₂ on TiO₂, *J. Phys. Chem. A.*, 123, 1311-1318,
584 <https://doi.org/10.1021/acs.jpca.8b11433>, 2019.

585 Martins-Costa, M., Anglada, J., Francisco, J., and Ruiz-Lopez, M.: Photochemistry of SO₂ at
586 the air-water interface: A source of OH and HOSO radicals, *J. Am. Chem. Soc.*, 140, 12341-
587 12344, <https://doi.org/10.1021/jacs.8b07845>, 2018.

588 Mauldin, R., Berndt, T., Sipila, M., Paasonen, P., Petaja, T., Kim, S., Kurten, T., Stratmann, F.,
589 Kerminen, V., and Kulmala, M.: A new atmospherically relevant oxidant of sulphur dioxide,
590 *Nature*, 488, 193-196, <https://doi.org/10.1038/nature11278>, 2012.

591 Mukuta, T., Fukazawa, N., Murata, K., Inagaki, A., Akita, M., Tanaka, S., Koshihara, S. Y., and
592 Onda, K.: Infrared vibrational spectroscopy of [Ru(bpy)₂(bpm)]²⁺ and [Ru(bpy)₃]²⁺ in the

593 excited triplet state, *Inorg. Chem.*, 53, 2481-2490, <https://doi.org/10.1021/ic402474t>, 2014.

594 Olson, E., Michalski, G., Welp, L., Valdivia, A., Larico, J., Pen, J., Fang, H., Gomez, K., and
595 Li, J.: Mineral dust and fossil fuel combustion dominate sources of aerosol sulfate in urban
596 Peru identified by sulfur stable isotopes and water-soluble ions, *Atmos. Environ.*, 260,
597 118482-118495, <https://doi.org/10.1016/j.atmosenv.2021.118482>, 2021.

598 Park, J. and Jang, M.: Heterogeneous photooxidation of sulfur dioxide in the presence of airborne
599 mineral dust particles, *RSC Adv.*, 6, 58617-58627, <https://doi.org/10.1039/c6ra09601h>,
600 2016.

601 Park, J., Jang, M., and Yu, Z.: Heterogeneous photo-oxidation of SO₂ in the presence of two
602 different mineral dust particles: Gobi and arizona dust, *Environ. Sci. Technol.*, 51, 9605-
603 9613, <https://doi.org/10.1021/acs.est.7b00588>, 2017.

604 Peng, Y., von Salzen, K., and Li, J.: Simulation of mineral dust aerosol with Piecewise Log-
605 normal Approximation (PLA) in CanAM4-PAM, *Atmos. Chem. Phys.*, 12, 6891-6914,
606 <https://doi.org/10.5194/acp-12-6891-2012>, 2012.

607 Prospero, J.: Long-range transport of mineral dust in the global atmosphere: Impact of African
608 dust on the environment of the southeastern United States, *Proc. Natl. Acad. Sci. U. S. A.*,
609 96, 3396-3403, <https://doi.org/10.1073/pnas.96.7.3396>, 1999.

610 Shao, J., Chen, Q., Wang, Y., Lu, X., He, P., Sun, Y., Shah, V., Martin, R. V., Philip, S., Song,
611 S., Zhao, Y., Xie, Z., Zhang, L., and Alexander, B.: Heterogeneous sulfate aerosol formation
612 mechanisms during wintertime Chinese haze events: air quality model assessment using
613 observations of sulfate oxygen isotopes in Beijing, *Atmos. Chem. Phys.*, 19, 6107-6123,
614 <https://doi.org/10.5194/acp-19-6107-2019>, 2019.

615 Shiraiwa, M., Ueda, K., Pozzer, A., Lammel, G., Kampf, C. J., Fushimi, A., Enami, S., Arangio,
616 A. M., Frohlich-Nowoisky, J., Fujitani, Y., Furuyama, A., Lakey, P. S. J., Lelieveld, J., Lucas,
617 K., Morino, Y., Poschl, U., Takahama, S., Takami, A., Tong, H., Weber, B., Yoshino, A., and
618 Sato, K.: Aerosol health effects from molecular to global scales, *Environ. Sci. Technol.*, 51,
619 13545-13567, <https://doi.org/10.1021/acs.est.7b04417>, 2017.

620 Sidebottom, H. W., Badcock, C. C., Jackson, G. E., Calvert, J. G., Reinhardt, G. W., and Damon,
621 E. K.: Photooxidation of sulfur dioxide, *Environ. Sci. Technol.*, 6, 72-79,
622 <https://doi.org/10.1080/00022470.1971.10469552>, 1972.

623 Solbrig, C. W. and Gidaspow, D.: Convective diffusion in a parallel plate duct with one catalytic
624 wall, laminar flow, first order reaction-part one, *Can. J. Chem. Eng.*, 45, 35-39,
625 [https://doi.org/10.1016/0304-5102\(89\)80197-X](https://doi.org/10.1016/0304-5102(89)80197-X), 1967.

626 Sumner, A. L., Menke, E. J., Dubowski, Y., Newberg, J. T., Penner, R. M., Hemminger, J. C.,
627 Wingen, L. M., Brauers, T. and Finlayson-Pitts, B. J. The nature of water on surfaces of
628 laboratory systems and implications for heterogeneous chemistry in the troposphere. *Phys.*
629 *Chem. Chem. Phys.*, 6, 604-613, <https://doi.org/10.1039/B308125G>, 2004.

630 Tohidi, R., Farahani, V., and Sioutas, C.: Real-time measurements of mineral dust concentration
631 in coarse particulate matter PM_{10-2.5} by employing a novel optical-based technique in Los
632 Angeles, *Sci. Total. Environ.*, 838, 156215-156226, <https://doi.org/10.1016/j.scitotenv.2021.156215>, 2022.

633
634 Urupina, D., Romanias, M. N., and Thevenet, F.: How relevant is it to use mineral proxies to

635 mimic the atmospheric reactivity of natural dust samples? A reactivity study using SO₂ as
636 probe molecule, *Minerals*, 11, 282-299, <https://doi.org/10.3390/min11030282>, 2021.

637 Urupina, D., Lasne, J., Romanias, M. N., Thiery, V., Dagsson-Waldhauserova, P., and Thevenet,
638 F.: Uptake and surface chemistry of SO₂ on natural volcanic dusts, *Atmos. Environ.*, 217,
639 116942-116959, <https://doi.org/10.1016/j.atmosenv.2019.116942>, 2019.

640 Usher, C., Michel, A., and Grassian, V.: Reactions on mineral dust, *Chem. Rev.*, 103, 4883-
641 4939, <https://doi.org/10.1021/cr020657y>, 2003.

642 Usher, C., Al-Hosney, H., Carlos-Cuellar, S., and Grassian, V.: A laboratory study of the
643 heterogeneous uptake and oxidation of sulfur dioxide on mineral dust particles, *J. Geophys.*
644 *Res-atmos.*, 107, 4713-4729, <https://doi.org/10.1029/2002jd002051>, 2002.

645 Wang, J., Li, J., Ye, J., Zhao, J., Wu, Y., Hu, J., Liu, D., Nie, D., Shen, F., Huang, X., Huang,
646 D. D., Ji, D., Sun, X., Xu, W., Guo, J., Song, S., Qin, Y., Liu, P., Turner, J. R., Lee, H. C.,
647 Hwang, S., Liao, H., Martin, S. T., Zhang, Q., Chen, M., Sun, Y., Ge, X., and Jacob, D. J.:
648 Fast sulfate formation from oxidation of SO₂ by NO₂ and HONO observed in Beijing haze,
649 *Nat. Commun.*, 11, 2844-2850, <https://doi.org/10.1038/s41467-020-16683-x>, 2020a.

650 Xu, M., Qiu, P., He, Y., Guo, S., Bai, Y., Zhang, H., Zhao, S., Shen X., Zhu, B., Guo, Q., Guo,
651 Z., Sulfur isotope composition during heterogeneous oxidation of SO₂ on mineral dust: The
652 effect of temperature, relative humidity, and light intensity. *Atmos. Res.*, 254, 105513,
653 <https://doi.org/10.1016/j.atmosres.2021.105513>, 2021.

654 Yao, M., Zhao, Y., Hu, M., Huang, D., Wang, Y., Yu, J. Z., and Yan, N.: Multiphase reactions
655 between secondary organic aerosol and sulfur dioxide: Kinetics and contributions to sulfate
656 formation and aerosol aging. *Environ. Sci. Technol. Lett.*, 6, 768-774,
657 <https://doi.org/10.1021/acs.estlett.9b00657>, 2019.

658 Ye, J., Abbatt, J. P. D., Chan, A. W. H.: Novel pathway of SO₂ oxidation in the atmosphere:
659 Reactions with monoterpene ozonolysis intermediates and secondary organic aerosol.
660 *Atmos. Chem. Phys.*, 18, 5549-5565, <https://doi.org/10.5194/acp-18-5549-2018>, 2018.

661 Wang, S., Zhou, S., Tao, Y., Tsui, W. G., Ye, J., Yu, J. Z., Murphy, J. G., McNeill, V. F., Abbatt,
662 J. P. D., and Chan, A. W. H.: Organic peroxides and sulfur dioxide in aerosol: Source of
663 particulate sulfate. *Environ. Sci. Technol.*, 53, 10695-10704, [https://doi.org/10.1021/acs.es](https://doi.org/10.1021/acs.est.9b02591)
664 [t.9b02591](https://doi.org/10.1021/acs.est.9b02591), 2019.

665 Wang, T., Liu, Y., Deng, Y., Fu, H., Zhang, L., and Chen, J.: The influence of temperature on
666 the heterogeneous uptake of SO₂ on hematite particles, *Sci. Total. Environ.*, 644, 1493-1502,
667 <https://doi.org/10.1016/j.scitotenv.2018.07.046>, 2018.

668 Wang, T., Liu, Y. Y., Deng, Y., Cheng, H. Y., Yang, Y., Li, K. J., Fang, X. Z., and Zhang, L. W.:
669 Irradiation intensity dependent heterogeneous formation of sulfate and dissolution of ZnO
670 nanoparticles, *Environ. Sci.: Nano*, 7, 327-338, <https://doi.org/10.1039/c9en01148j>, 2020b.

671 Wang, Z., Wang, T., Fu, H., Zhang, L., Tang, M., George, C., Grassian, V. H., and Chen, J.:
672 Enhanced heterogeneous uptake of sulfur dioxide on mineral particles through modification
673 of iron speciation during simulated cloud processing, *Atmos. Chem. Phys.*, 19, 12569-12585,
674 <https://doi.org/10.5194/acp-19-12569-2019>, 2019.

675 Yang, N., Tsona, N. T., Cheng, S., Li, S., Xu, L., Wang, Y., Wu, L., and Du, L.: Competitive
676 reactions of SO₂ and acetic acid on α -Al₂O₃ and CaCO₃ particles, *Sci. Total. Environ.*, 699,

677 134362-134370, <https://doi.org/10.1016/j.scitotenv.2019.134362>, 2020.

678 Yang, W., Ma, Q., Liu, Y., Ma, J., Chu, B., and He, H.: The effect of water on the heterogeneous
679 reactions of SO₂ and NH₃ on the surfaces of α-Fe₂O₃ and γ-Al₂O₃, *Environ. Sci.: Nano*, 6,
680 2749-2758, <https://doi.org/10.1039/c9en00574a>, 2019.

681 Zhang, P., Chen, T., Ma, Q., Chu, B., Wang, Y., Mu, Y., Yu, Y., and He, H.: Diesel soot
682 photooxidation enhances the heterogeneous formation of H₂SO₄, *Nat. Commun.*, 13, 5364-
683 5372, <https://doi.org/10.1038/s41467-022-33120-3>, 2022.

684 Zhang, R., Gen, M., Huang, D., Li, Y., and Chan, C.: Enhanced sulfate production by nitrate
685 photolysis in the presence of halide ions in atmospheric particles, *Environ. Sci. Technol.*,
686 54, 3831-3839, <https://doi.org/10.1021/acs.est.9b06445>, 2020a.

687 Zhang, T., Yang, W., Han, C., Yang, H., and Xue, X.: Heterogeneous reaction of ozone with
688 syringic acid: Uptake of O₃ and changes in the composition and optical property of syringic
689 acid, *Environ. Pollut.*, 257, 113632-113638, <https://doi.org/10.1016/j.envpol.2019.113632>,
690 2020b.

691 Zhang, X., Zhuang, G., Chen, J., Wang, Y., Wang, X., An, Z., and Zhang, P.: Heterogeneous
692 reactions of sulfur dioxide on typical mineral particles, *J. Phys. Chem. B*, 110, 12588-12596,
693 <https://doi.org/10.1021/jp0617773>, 2006.

694 Zhang, Y., Bao, F., Li, M., Chen, C., and Zhao, J.: Nitrate-enhanced oxidation of SO₂ on mineral
695 dust: A vital role of a proton, *Environ. Sci. Technol.*, 53, 10139-10145,
696 <https://doi.org/10.1021/acs.est.9b01921>, 2019.

697 Zhang, Y., Bao, F., Li, M., Xia, H., Huang, D., Chen, C., and Zhao, J.: Photoinduced uptake
698 and oxidation of SO₂ on Beijing urban PM_{2.5}, *Environ. Sci. Technol.*, 54, 14868-14876,
699 <https://doi.org/10.1021/acs.est.0c01532>, 2020c.

700